J Supercond Nov Magn (2018) 31:1607–1613
https://doi.org/10.1007/s10948-017-4351-7

ORIGINAL PAPER

Magnetic and Structural Properties of $SrFe_{12-x}Cr_xO_{19}$ ($x = 0, 0.25, 0.5, 0.75, 1$) Hexaferrite Powders Obtained by Sol–Gel Auto-Combustion Method

Ebrahim Roohani[1,3] · Hadi Arabi[2] · Reza Sarhaddi[1] · Ameneh Shabani[1]

Received: 28 August 2017 / Accepted: 13 September 2017 / Published online: 9 October 2017

Abstract The crystalline structure and magnetic properties of chromium substituted hexagonal strontium ferrite, $SrFe_{12-x}Cr_xO_{19}$ ($x = 0, 0.25, 0.5, 0.75, 1$), nanoparticles have been investigated by means of X-ray diffraction (XRD), transmission electron microscopy (TEM), Fourier transform infrared spectroscopy (FT-IR), and vibrating sample magnetometer (VSM). These materials were prepared by the chemical sol–gel auto-combustion method. From the structural analysis, it was observed that the non-magnetic phase α-Fe_2O_3 appears after $x \geq 0.5$ and remains to be a hexagonal magnetoplumbite phase for $x < 0.5$. Various parameters such as lattice constants (a and c) were calculated from the XRD data. The coercively H_c initially decreases and then increases with increasing chromium concentration. The saturation magnetization exhibits an increase as the chromium content increases up to ($x = 0.25$) and then decreases with increase in the Cr content ion from 75.19 to 61.66 emu/g due to the substitution of Fe^{3+} ions by less magnetic Cr^{3+} ions. Furthermore, M_r continually decreases with increase in the Cr content.

Keywords Magnetoplumbite · Cr substitution · Sol-gel method · Magnetic properties · Saturation magnetization

1 Introduction

Strontium hexaferrite belongs to a hexagonal M-type magnetoplumbite structure $MFe_{12}O_{19}$, where M = Sr, Ba, Pb, and space group $P6_3/mmc$ ferrimagnetic material with easy magnetization in the direction of c-axis [1–3]. M-type hexaferrites have attracted considerable attention because of chemically stability, low production price, high Curie temperature (720 K), magnetocrystalline anisotropy along c-axis, high-saturation magnetization and high coercivity, due to these beneficial properties, the M-type hexaferrites have been widely used in the permanent magnetic material, high-density magnetic recording media, sensors, telecommunication, microwave devices, ceramic magnets in loud speakers, and the rotors in small DC motors [1–5]. Strontium hexaferrite nanoparticles can be prepared by several preparation techniques including the solid-state method, ball milling, hydrothermal method, co-precipitation techniques, the traditional sol-gel process, and sol-gel auto-combustion method [2]. Among these different methods, the sol–gel auto-combustion method has attracted considerable attention because of its relatively simple synthesis program [6].

In order to improve the inherent magnetic properties of M-type hexaferrite, and to make these materials suitable for different applications, many researchers have focused on modifying the magnetic properties of strontium ferrite by the substitution Fe^{3+} ions with other cations or cation combinations such as Co^{2+}, Ni^{2+}, Al^{3+}, Zr–Mn, Mg–Zr, and Pr–Ni [7–11]. In the present study, the substitution of chromium trivalent ion (Cr^{3+}) with ($x = 0, 0.25, 0.5, 0.75, 1$) contents on the Fe site of $SrFe_{12}O_{19}$ compound, which were

✉ Ebrahim Roohani
ebrahimroohani@yahoo.com

[1] Magnetism and Superconducting Research Laboratory, Department of Physics, University of Birjand, P.O. Box 97175-615, Birjand, Iran

[2] Department of Physics, Faculty of Science, Ferdowsi University of Mashhad, Mashhad, Iran

[3] Department of Engineering, Bardaskan Branch, Islamic Azad University, Bardaskan, Iran

prepared by sol–gel auto-combustion method have been investigated. The main aim of this study is to synthesize chromium-substituted hexaferrite nanosize materials by a suitable methodology and to evaluate the possible changes in its structure and magnetic properties.

2 Experimental Details

2.1 Materials

Strontium nitrate anhydrous ($Sr(NO_3)_2$), iron (III) nitrate nonahydrate ($Fe(NO_3)_3.9H_2O$) and chromium (III) nitrate nonahydrate ($Cr(NO_3)_3.9H_2O$) as inorganic reactants; citric acid ($C_6H_8O_7$) as complexing agent, ammonium hydroxide as a neutralizing agent, and double-distilled water as solvent were used to prepare Cr-substituted strontium hexaferrite nanoparticles by sol-gel auto-combustion method.

2.2 Sample Synthesis

In this study, $SrFe_{12-x}Cr_xO_{19}$ ($x = 0 - 1$) M-type hexagonal ferrites were prepared by sol-gel auto-combustion method. The aqueous sol was prepared by dissolving $Fe(NO_3)_3.9H_2O$ (Merck 99%), $Sr(NO_3)_2$ (Merck 99%), and $Cr(NO_3)_3.9H_2O$ (Merck 99%), according to appropriate stoichiometric proportion, in double-distilled water and then mixed together by constant stirring on a hotplate at 50 °C. Then, citric acid was added to the solution (citric acid to total metal ions molar ratio of 1:1) for the enhancement of nitrates dissolution and subsequently stirred for 45 min at 70 °C. Afterward, the pH of the final solution was adjusted to about 7 by adding ammonium. The dark brown solution were stirred and heated for several hours at 80 °C until the sol turned into a dried gel. The obtained gel was heated at 250 °C for 1 h to eliminate the residual organic compound. The combustion reaction equation of the gels can be described simply as the following:

$$Sr(NO_3)_2 + x\,Cr(NO_3)_3.9H_2O + (12 - x)\,Fe(NO_3)_3.9H_2O + y C_6H_8O_7 + z\,NH_4OH + H_2O \xrightarrow{80°C} \text{Sol–gels}$$

$$\text{Sol–gels} \xrightarrow{\text{Air ignition}} SrFe_{12-x}Cr_xO_{19} + m\,Co_2 + n\,NO + p\,H_2O$$

Finally, the as-burnt powder was ground and then calcined at 1000 °C in air for 5 h with a heating rate of 5 °C/min to remove any organic residue and to form the hexaferrite phase. A schematic diagram of the synthesis process is showed in Fig. 1.

2.3 Powders Characterization

Fourier transform infrared (FT-IR) spectra of powders (as-burnt and calcined) were recorded by a Shimadzu FTIR 4300 spectrometer in a wavenumber range of 400–4000 cm^{-1}. The crystallographic properties of the powders were characterized by the D8 Advance (Bruker) X-ray diffractometer with Cu–K_α radiation (the wavelength $\lambda = 1.54056$ Å) and the 2θ range from 25° to 75°. Transmission electron

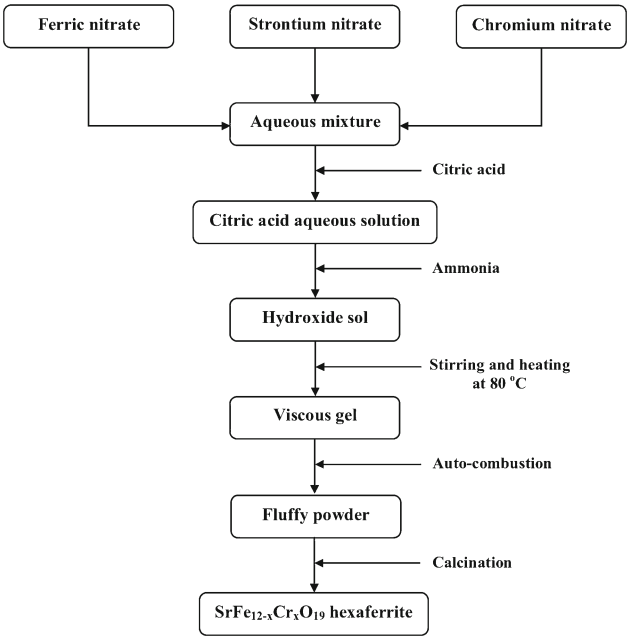

Fig. 1 Schematic diagram of synthesis process

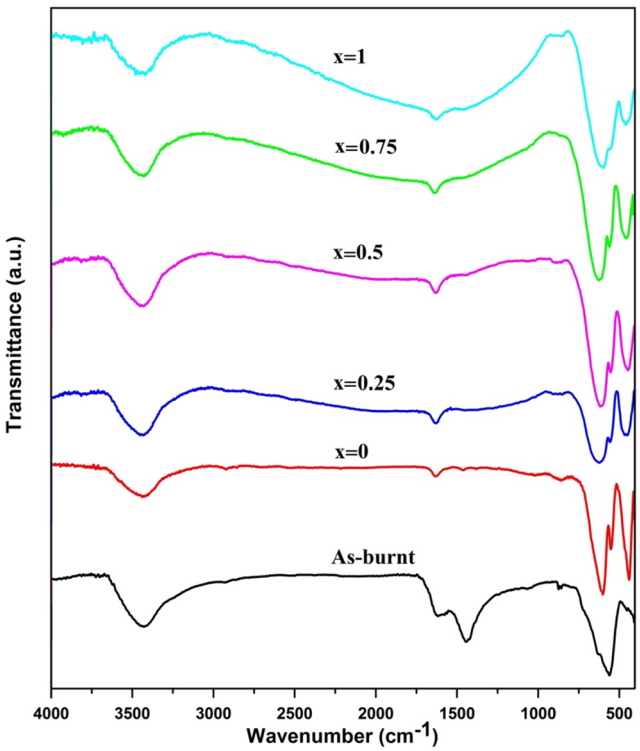

Fig. 2 FT-IR patterns of $SrFe_{12-x}Cr_xO_{19}$ ($x = 0$–1) calcined powders together with as-burnt $SrFe_{12}O_{19}$ sample

microscopy (TEM) images were obtained by using an LEO 912 AB system operating at 120 kV. The magnetic properties were measured by a vibrating sample magnetometer (VSM, Lake Shore 7404) with a maximum field strength of 20 kOe. All the measurements were performed at room temperature.

3 Results and Discussion

3.1 FT-IR Analysis

The FT-IR spectra of the as-burnt and calcined samples at 1000 °C for 5 h in the range of 400–4000 cm^{-1}, are shown in Fig. 2. As can be seen, for the as-burnt sample the characteristics of absorption of C–N=O are at wave number 562 cm^{-1}, C–C at 874 cm^{-1}, C–O at 1104 cm^{-1}, C–H at 1444 cm^{-1}, C=O at 1617 cm^{-1}, and O–H at 3425 cm^{-1}, respectively [12, 13]. Moreover, for calcined samples, three characteristics of vibration frequencies in the range of 440–450, 550–560, and 600–625 cm^{-1} appear. These frequency modes, which correspond to the formation of octahedral (440–450 cm^{-1}) and tetrahedral (550–560, 600–625 cm^{-1}) clusters, confirm the presence of metal-oxygen (M–O) stretching bands in strontium hexaferrite [14–16]. In addition, due to the shorter bond length of tetrahedral clusters, these vibrational modes are higher than that of octahedral clusters [16]. There is also a minor absorption peak around 1630 cm^{-1}, which was due to symmetric and asymmetric vibrations of the coordinated carboxylate groups [17]. Furthermore, the absorption peak at the range of 3418–3430 cm^{-1} is associated with the hydroxyl of bonds (−OH) [17]. It can be also observed that with the increase of Cr^{3+} ion content (i.e., x), the value of FT-IR characteristic frequencies for $SrFe_{12-x}Cr_xO_{19}$ samples were shifted to a higher wavenumber due to Cr^{3+} ions with a lighter atomic weight than Fe^{3+} ions and the wavenumber being inversely proportional to the atomic weight [7]. According to the mentioned results, it can be concluded that with the calcination of as-burnt powders at 1000 °C, all of the organic compounds were completely eliminated; consequently, bonds between metals and oxygen formed, which resulted in formation of crystal structure. From the comparison of the un-doped and doped samples, it is observed that chromium substitution

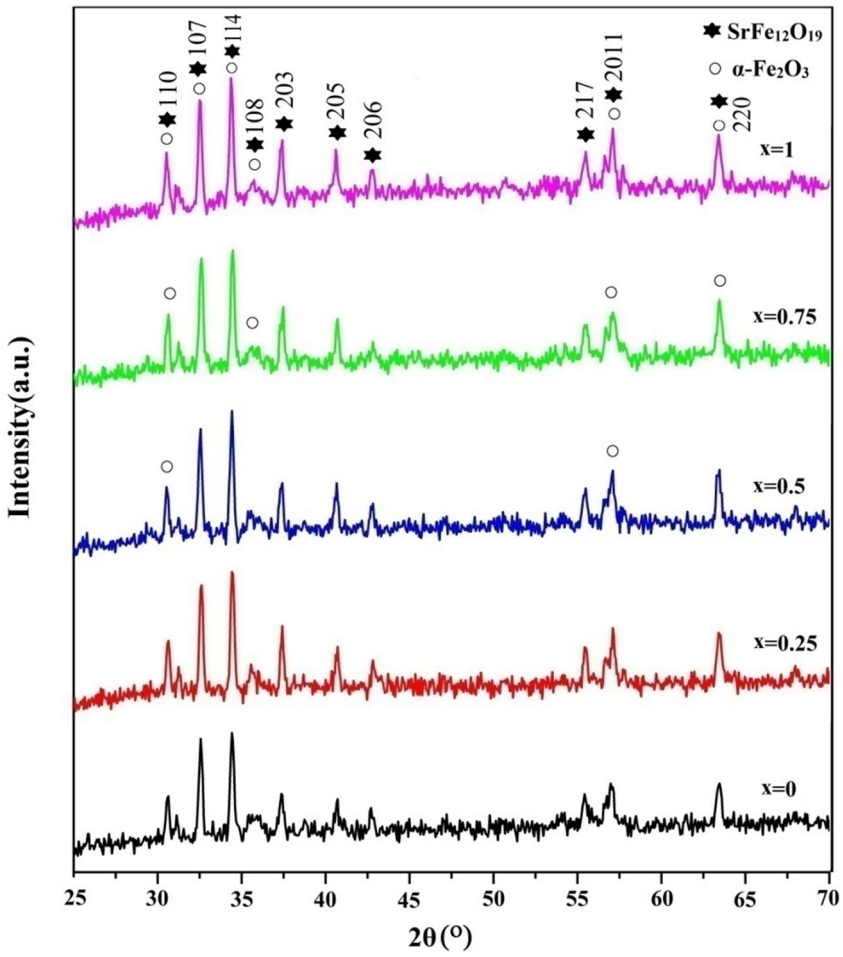

Fig. 3 XRD patterns of $SrFe_{12-x}Cr_xO_{19}$ ($x = 0$–1) powders

Table 1 The structural parameters of $SrFe_{12-x}Cr_xO_{19}$ ($x = 0$–1) samples

x	a (Å)	c (Å)	c/a	ρ_{X-ray} (g cm^{-3})	Volume (Å^3)	Crystallite size (nm)
0	5.863	23.012	3.924	5.15	685.508	48
0.25	5.855	22.933	3.916	5.17	681.292	42
0.5	5.845	22.928	3.922	5.18	678.818	38
0.75	5.843	22.873	3.914	5.20	676.727	36
1	5.840	22.868	3.915	5.19	675.884	35

in the structure of strontium hexaferrite does not have a significant effect on the bonding position.

3.2 XRD Analysis

X-ray diffraction patterns of $SrFe_{12-x}Cr_xO_{19}$, ($x = 0, 0.25, 0.5, 0.75, 1$) nanoparticles calcined at 1000 °C for 5 h in air are shown in Fig. 3. The main diffraction peaks related to strontium M-type hexaferrite were appeared at 2θ of 30.36° , 32.32°, 34.17°, 37.13°, 40.34° , 55.18°, 56.73°, and 63.13°. These diffraction planes were respectively ascribed to (110), (107), (114), (203), (205), (217), (2011), and (220) [18, 19]. All of these diffraction planes are relevant to the diffraction peaks of M-type hexaferrite (JCPDS card (#33-1340)). Furthermore, an additional peaks corresponding to extra phase of α-Fe_2O_3 also appeared [18, 19]. The appearance of a second phase of α-Fe_2O_3 probably due to the fact that the calcination temperature was low or the calcination time was too short. Furthermore, It is reported that the single phase of pure M-type hexaferrites can be obtained at higher sintering temperatures >1000 °C [19, 20].

As can be seen in the X-ray diffraction patterns, the intensity of α-Fe_2O_3 peaks increased with increase in the concentration of chromium content. It means that the substitution of Fe^{3+} ions by Cr^{3+} ions in the M-type hexagonal lattice is imperfect [19]. The average crystallites size (D) of the samples were calculated from X-ray line broadening of the reflection of (114), (107), and (203) by using Debye–Scherrer's equation and were found to be in the range of 35 to 48 nm. In addition, The lattice parameters (a and c), cell volume (v), and X-ray density (ρ_{X-ray}) have been calculated from the XRD data using the following equations:

$$D = \frac{0.89\lambda}{\beta \cos\theta}, \tag{1}$$

$$\frac{1}{d^2} = \frac{4}{3}\left(\frac{h^2 + hk + k^2}{a^2}\right) + \frac{l^2}{c^2}, \tag{2}$$

$$V = \frac{\sqrt{3}}{2}a^2 c, \tag{3}$$

$$\rho_{\text{X-ray}} = \frac{ZM}{N_A V}, \tag{4}$$

where λ is the wavelength of the X-ray radiation, θ is the diffraction angle, and β is the full width at half maximum (FWHM)), hkl are the corresponding indices of each line in the pattern, Z is the number of formula units in a unit cell, M is the molecular mass of the sample, and N_A is the Avogadro's number [7, 19, 20]. The obtained results are listed in Table 1.

It can be seen (4) that the value of X-ray density ($\rho_{\text{X-ray}}$) directly depends on the molecular weight of the sample and cell volume. The value of X-ray density slightly increases from 5.15 to 5.20 g cm^{-3} with the increase in concentration of the Cr^{3+} ion (Table 1), which is due to insignificant decrease in the cell volume of the respective samples [21]. As can be seen, the lattice parameters (a and c) decrease with increasing x value. As we know, the radius of Cr^{3+} ions (0.63 Å) is almost equal to that of radius of Fe^{3+} ions

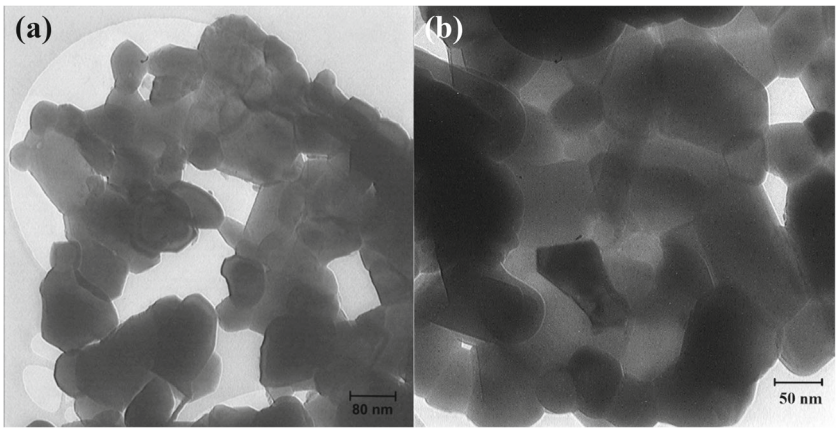

Fig. 4 TEM images of $SrFe_{12-x}Cr_xO_{19}$ nanoparticles **a** x = 0 and **b** x = 1

(0.64 Å) [22]. Therefore, the change in the lattice parameters is not due to the effect of size but might be due to the change of exchange energy after Cr^{3+} ion substitution [22]; however, the detailed mechanism needs to be further studied. From the results of Table 1, it is observed that the "c/a" values were calculated for the $SrFe_{12-x}Cr_xO_{19}$ ($x = 0 - 1$) samples, ranged from 3.914 to 3.924.

3.3 TEM Analysis

Figure 4 shows the TEM images of $SrFe_{12-x}Cr_xO_{19}$ ($x = 0, 1$) particles prepared by sol–gel auto-combustion method. As it is observed from Fig. 4, the average grain size of all the substituted hexaferrites is almost similar, and they adhere each other due to their magnetic attraction between the particles [23]. These nanoparticles are hexagonal platelet-like crystals which are also observed for $BaFe_{12}O_{19}$ and $PbFe_{12}O_{19}$ hexaferrites and the average size of the $SrFe_{12-x}Cr_xO_{19}$ ($x = 0, 1$) particles is in the range 50–65 nm.

3.4 Magnetic Analysis

The hysteresis loops for $SrFe_{12-x}Cr_xO_{19}$ ($x = 0 - 1$) which were measured at room temperature are shown in Fig. 5. It has been reported that the width and the shape of the hysteresis loop depend on different parameters such as chemical composition, cation distribution, grain size, and porosity [24]. From Fig. 5, it is observed that the magnetization did not saturate because the maximum magnetic field (20 kOe) of VSM used in the present study are unable to saturate the samples. Therefore, the saturation magnetization was determined from the extrapolation of the plot M versus $1/H$ [7]. The obtained results were presented in Table 2.

The values of saturation magnetization (M_s), remanence (M_r), squareness ratio (M_r/M_s), and coercivity (H_c) were calculated from the hysteresis loops and listed in Table 2. As can be seen (Fig. 6), the saturation magnetization at first slightly increased and reaches a maximum value at $x = 0.25$; which express that a small amount of the chromium doping leads to the increase of saturation magnetization. This increase probably due to the fact that the magnetic moment of Cr^{3+} (3 μ_B) ion is smaller than that of Fe^{3+} (5 μ_B) ion [22, 25]. It is well known that in a unit cell of strontium hexaferrite, the Fe^{3+} ions are distributed in five different sublattice sites: (2a, 12k, and 2b) sites having spin up direction, and ($4f_1$ and $4f_2$) sites having spin down [7]. When substitution occurred ($x \leq 0.25$) the number of Cr^{3+} ions entering $4f_2$ site (spin-down) is more than that of in 12k and 2a sites (spin-up) [22, 25]; therefore, the saturation magnetization increased while for $x > 0.25$; the saturation magnetization decreased continuously. These changes may be due to the two reasons: the first one is due to the appearance of non-magnetic phase α-Fe_2O_3 and the second one may be also due to the fact that at high doping content ($x > 0.25$), Cr^{3+} ion substitutes Fe^{3+} ion in 12k and 2a sites having spin-up [22]. Therefore, as mentioned above, the saturation magnetization decreased because chromium saturation magnetization is less than iron magnetization [25]. On the other hand, the value of coercivity at first, decreases rapidly and reaches a minimum at $x = 0.5$; then, H_c increases slightly (Fig. 6). It has been reported that the coercivity is affected by important

Table 2 The magnetic parameters of $SrFe_{12-x}Cr_xO_{19}$ ($x = 0 - 1$) samples

x	M_r (emu/g)	M_s (emu/g)	M_r/M_s	H_c(Oe)
0	33.50	74.26	0.451	5672
0.25	32.323	75.192	0.429	1696
0.5	29.356	69.457	0.422	1384
0.75	29.75	67.047	0.443	2242
1	27.436	61.663	0.444	2337

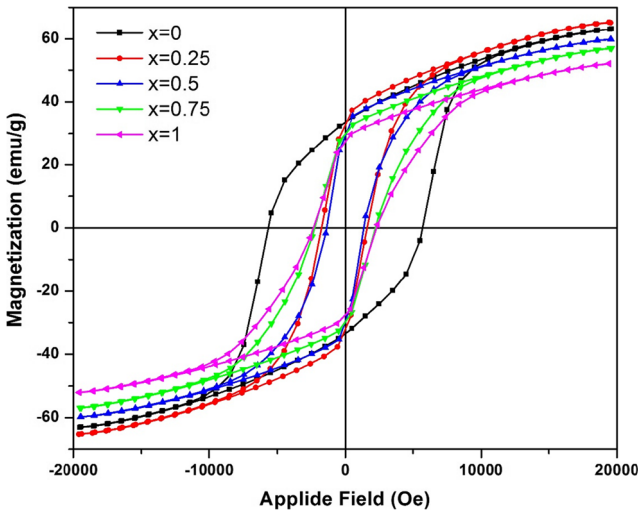

Fig. 5 Hysteresis loops of $SrFe_{12-x}Cr_xO_{19}$ ($x = 0$–1) powders

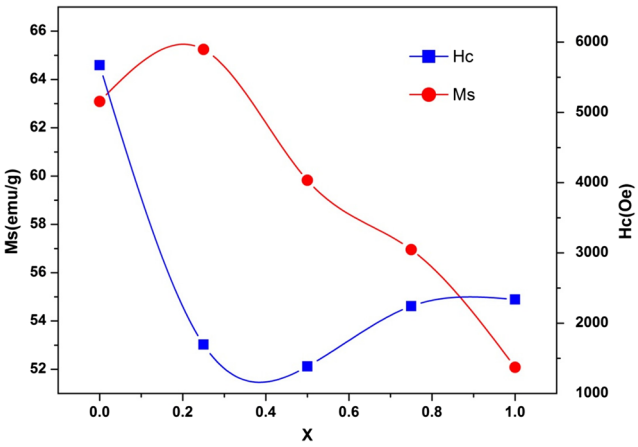

Fig. 6 H_c and M_s of $SrFe_{12-x}Cr_xO_{19}$ samples as a function of x

parameters such as particle size, ion substitution, morphology, interface structure, crystal defects, magnetocrystalline anisotropy, and strain [26]. However, among these parameters, the ion substitution and particle size are undoubtedly two of the most important parameters [26]. In this research, the decrease of coercivity with increase in Cr^{3+} concentration up to $x = 0.5$ may be due to decrease in magnetocrystalline anisotropy. Furthermore, the increase of H_c at the high doping content may be due to the appearance of non-magnetic phase α-Fe_2O_3 [22]. The squareness ratio (SQR) is calculated from the magnetic data and their values are listed in Table 2. It has been reported that large squareness ratio is favored in many applications such as the magnetic recording media and permanent magnets [7]. In the present study, the squareness ratios are found in the range of 0.422–0.451, indicating that materials are in single magnetic domain.

4 Conclusion

The sol–gel auto-combustion method has been successfully employed for the synthesis of chromium-substituted strontium hexaferrite nanomaterials. The X-ray diffraction patterns of samples confirmed the formation of hexagonal magnetoplumbite phase with the space group of $P6_3/mmc$. However, the small amounts of impurity phases (α-Fe_2O_3) also appeared. The FT-IR spectra of samples after calcination process showed three absorption peaks in the range of 440–450, 550–560, and 600–625 cm^{-1} originated from the metal oxygen (M–O) stretching band in strontium hexaferrite. The TEM images showed nearly hexagonal platelet shape for strontium ferrite nanoparticles. The magnetic properties including M_s, M_r, SQR, and H_c were investigated. The saturation magnetization of chromium-substituted Sr hexaferrite at first increases slightly and then decreases continuously due to the appearance of non-magnetic phase α-Fe_2O_3. The coercivity of the samples at first, decreases rapidly and reaches a minimum at $x = 0.5$, then increases slightly.

Acknowledgments The authors would like to thank the "Iranian Nanotechnology Initiative Council" for their financial support.

References

1. Dho, J., Lee, E.K., Park, J.Y., Hur, N.H.: Effects of the grain boundary on the coercivity of barium ferrite $BaFe_{12}O_{19}$. J. Magn. Magn. Mater. **285**, 164–168 (2005)
2. Zi, Z.F., Sun, Y.P., Zhu, X.B., Yang, Z.R., Dai, J.M., Song, W.H.: Structural and magnetic properties of $SrFe_{12}O_{19}$ hexaferrite synthesized by a modified chemical co-precipitation method. J. Magn. Magn. Mater. **320**, 2746–2751 (2008)
3. Wang, Y., Li, Q., Zhang, C., Li, B.: Effect of Fe/Sr mole ratios on the formation and magnetic properties of $SrFe_{12}O_{19}$ microtubules prepared by sol–gel method. J. Magn. Magn. Mater. **321**, 3368 (2009)
4. Went, J.J., Ratheneau, G.W., Gorter, E.W., Van Oosterhout, G.W.: Ferroxdure, A class of new permanent magnet materials. Philips Tech. Rev. **13**, 194–208 (1951)
5. Pullar, R.C.: Hexagonal ferrites: a review of the synthesis, properties and applications of hexaferrite ceramics. Prog. Mater. Sci. **57**, 1191–1334 (2012)
6. Ghobeiti Hasab, M., Seyyed Ebrahimi, S.A., Badiei, A.: An investigation on physical properties of strontium hexaferrite nanopowder synthesized by a sol–gel auto-combustion process with addition of cationic surfactant. J. Eur. Ceram. Soc. **27**, 3637–3640 (2007)
7. Roohani, E., Arabi, H., Sarhaddi, R., Sudkhah, S.: M-type strontium hexaferrite nanoparticles prepared by sol-gel auto-combustion method: the role of Co substitution in structural, morphological, and magnetic properties. J. Supercond. Nov. Magn. **30**, 1599–1608 (2017)
8. Roohani, E., Arabi, H., Sarhaddi, R.: Influence of nickel substitution on crystal structure and magnetic properties of strontium ferrite preparation via sol-gel auto-combustion route. International Journal of Modern Physics B. https://doi.org/10.1142/1142/S0217979217502711X
9. Iqbal, M.J., Ashiq, M.N.: Comparative studies of $SrZr_x$ Mn_x $Fe_{12-2x}O19$ nanoparticles synthesized by co-precipitation and sol–gel combustion methods. Scr. Mater. **56**, 145–148 (2007)
10. Sharbatia, A., Choopani, S., Azar, A.-M., Senna, M.: Structure and electromagnetic behavior of nanocrystalline $SrMg_xZr_xFe_{12-2x}O_{19}$ in the 8–12GHz frequency range. Solid State Commun. **150**, 2218–2222 (2010)
11. Iqbal, M.J., Farooq, S.: Impact of Pr–Ni substitution on the electrical and magnetic properties of chemically derived nanosized strontium–barium hexaferrites. J. Alloys Compd. **505**, 560–567 (2010)
12. Zhang, W., Tang, H., Peng, B., Zhang, W.: Influence of citric acid on the morphology and magnetic properties of barium ferrite thin films. Appl. Surface Sci. **257**, 176–179 (2010)
13. Naseri, M.G., Saion, E.B., Ahangar, H.A., Hashim, M., Shaari, A.H.: Powder Technol. **212**, 80 (2011)
14. Xie, T., Xu, L., Liu, C.: Synthesis and properties of composite magnetic material $SrCo_xFe_{12-x}O_{19}$ (x = 0-0.3). Powder Technol. **232**, 87–92 (2012)
15. Roohani, E., Arabi, H., Sarhaddi, R., Shabani, S.S.: Effect of annealing temperature on structural and magnetic properties of strontium hexaferrite nanoparticles synthesized by sol-gel auto-combustion method. Int. J. Mod. Phys. B **29**, 1550190 (2015)
16. Singhal, S., Namgyal, T., Singh, J., Chandra, K., Bansal, S.: A comparative study on the magnetic properties of $MFe_{12}O_{19}$ and $MAlFe_{11}O_{19}$ (M = Sr, Ba and Pb) hexaferrites with different morphologies. Ceram. Int. **37**, 1833–1837 (2011)
17. Kong, S., Zhang, P., Wen, X., Pi, P., Cheng, J., Yang, Z., Hai, J.: Influence of surface modification of $SrFe_{12}O_{19}$ particles with oleic acid on magnetic microsphere preparation. Particuology **6**, 185–190 (2008)
18. Rashad, M.M., Ibrahim, I.A.: Improvement of the magnetic properties of barium hexaferrite nanopowders using modified co-precipitation method. J. Magn. Magn. Mater. **323**, 2158–2164 (2011)
19. Ihsan Ali, M.U., Islam M.S., Ahmad, A.M., Asif Iqbal, M.: Structural, electrical, and microstructure properties of nanostructured calcium doped Ba-hexaferrites synthesized by sol-gel method. J. Supercond. Nov. Magn. **26**, 3277–3286 (2013)

20. Zargar Shoushtari, M., Mousavi Ghahfarokhi, S.E., Ranjbar, F.: A study of the morlogical properties of $SrFe_{12-x}Co_xO_{19}$ (x = 0, 0.1, 0.2) hexaferrite nanoparticles. J. Supercond. Nov. Magn. **28**, 1601–1609 (2015)
21. Iqbal, M.J., Farooq, S.: Extraordinary role of Ce–Ni elements on the electrical and magnetic properties of Sr–Ba M-type hexaferrites. Mater. Res. Bullet. **44**, 2050–2055 (2009)
22. Jauhar, S., Singh, J., Chandra, K., Bansal, S., Singhal, S.: Structural, morphological, magnetic and optical properties of chromium substituted strontium ferrites, $SrCr_xFe_{12-x}O_{19}$ (x = 0.5, 1.0, 1.5, 2.0 and 2.5) annealed with potassium halides. Powder Technol. **212**, 193–197 (2011)
23. Lee, S.-w., Drwiega, J., Mazyck, D., Wu, C.-Y., Sigmund, W.M.: Synthesis and characterization of hard magnetic composite photocatalyst—barium ferrite/silica/titania. Mater. Chem. Phys. **96**, 483–488 (2006)
24. Ahmad, M., Ali, I., Aen, F., Islam, M.U., Ashiq, M.N., Atiq, S., Ahmad, W., Rana, M.U.: Effect of sintering temperature on magnetic and electrical properties of nano-sized Co_2W hexaferrites. Ceram. Int. **38**, 1267–1273 (2012)
25. Fan, Q., Cheng, H., Huang, K., Wang, J., Li, R., Jiao, Y.: Doping effect on crystal structure and magnetic properties of chromium-substituted strontium hexaferrite nanoparticles. J. Magn. Magn. Mater. **294**, 281–286 (2005)
26. Liu, M., Shen, X., Song, F., Xiang, J., Meng, X.: Microstructure and magnetic properties of electrospun one-dimensional Al^{3+}-substituted $SrFe_{12}O_{19}$ nanofibers. J. Solid State Chem. **184**, 871–876 (2011)